

Mechanism of Luminescence Ring Pattern Formation in Quantum Well Structures: Optically-Induced In-Plane Charge Separation

R. Rapaport*,¹ Gang Chen*,¹ D. Snoke*,² Steven H. Simon,¹ Loren Pfeiffer,¹ Ken West,¹ Y. Liu,² and S. Denev²

¹*Bell Laboratories, Lucent Technologies,
600 Mountain Avenue, Murray Hill, New Jersey 07974*

²*Department of Physics and Astronomy,
University of Pittsburgh, 3841 O'Hara St., Pittsburgh, PA 15260*

* These authors have equal contributions.

About a year ago, two independent experiments[1, 2], imaging indirect exciton luminescence from doped double quantum wells under applied bias and optical excitation, reported a very intriguing observation: under certain experimental conditions, the exciton luminescence exhibits a ring pattern with a dark region in between the center excitation spot and the luminescent ring that can extend more than a millimeter from the center spot. Initial speculations on the origin of this emission pattern included supersonic ballistic transport of excitons due to their dipole-dipole repulsion and Bose superfluidity of excitons. In this paper we show that the ring effect is also observed in single quantum well structures, where only direct excitons exist. More importantly, we find that these experimental results are quantitatively explained by a novel coupled 2D electron-hole plasma dynamics, namely, photoinduced in-plane charge separation. This charge separation explains extremely long luminescence times that may be more than a microsecond for the ring — orders of magnitude longer than the emission lifetime of the excitons in the center spot. This method of continuously creating excitons may result in a highly dense exciton gas which is also well thermalized with the lattice (since the particles can cool over the very long luminescence time after their hot optical creation), thus opening up opportunities for a detailed study of quantum statistics. The in-plane separation of the charges into positive and negative regions, with a sharp interface between them is an interesting new example of nonequilibrium dynamics and pattern formation.

Butov et. al. [1] and Snoke et. al. [2] independently studied the emission from a modulation doped double quantum well (QW) structures under optical excitation from a tightly focused laser beam. When voltage is applied in the growth direction, emission is observed from indirect excitons — bound states of a single electron in one QW with a single hole in the other. Imaging the spatial distribution of this emission reveals a surprising pattern: in addition to the expected emission at the excitation spot, an emission ring is seen at large radial distances, with a dark region in between the center spot and the ring. The radius of the ring emission depends on the excitation power. An example of such an emission pattern is shown in Figure 1a. This striking effect calls for a consistent explanation of its underlying physical origin, which is the main purpose of this paper. Initial speculations based

on various exciton transport mechanisms and macroscopically coherent excitonic effects are inconsistent with many experimental results [3]. It is obvious that there is transport of particles from the excitation spot to the remote ring over macroscopic distances. However, in order to understand this effect, there are a few key questions one needs to address: (a) what types of particles or quasi-particles are being transported through the dark region to the ring location and what is the role of excitons in the transport and in the emission compared to that of free carriers? (b) what is the driving force for this unique transport?

One of the first key clues for solving this problem is our observation that identical ring patterns are also seen in single quantum well structures (see below), as opposed to the double QW structures studied in the initial reports [1, 2]. In our structure, there are only direct excitons (bound states of a single electron and a single hole in the *same* QW), which implies that the effect does not depend on the specific characteristics of indirect excitons (such as long lifetimes) as was suggested previously. Another important clue can be found in the observed excitation energy threshold of the ring formation as shown in Figure 1b: the ring easily forms only with photoexcitation energies which are above the AlGaAs barrier bandgap energy. This implies that the photogenerated hot carriers are a crucial ingredients in the ring formation and that the effect depends on the structure as a whole and not only on the local QW region. Since it is known that in modulation doped structures, optical excitation above the barriers can lead to depletion of electrons [4], it is interesting to ask whether the mechanism responsible for the ring formation has to do with such optical depletion.

It is then sensible to obtain further insight into the above mentioned questions by performing careful spectroscopic studies. The lineshapes, linewidths, and energies of the emission from the center spot and the ring are very good local probes of the carrier density distributions in the QW plane. In particular, excitonic emission lines characteristic of low densities should be significantly narrower, more symmetric, and blue shifted compared to emission resulting from recombination of free electron-hole plasmas of high densities [5].

Figure 2a-c show the ring pattern from our single well sample at various different excitation powers. As shown in more detail in Figure 3a, the ring radius grows (sublinearly) with increasing excitation power above a certain critical threshold for ring creation. Figure 2g-i show the center spot and ring PL spectra corresponding to Figure 2a-c. The detailed behavior of the spectral linewidth and energy as a function of excitation power is shown in Figure 3b-c for both the center spot and the ring. From Figure 3b-c, we see the following

trend: At low excitation power, there is no ring and the emission of the center spot is broad, asymmetric, and red shifted (see also Figure 2g), which would be characteristic of emission from a region with a high density of dissociated charge carriers (an electron-hole plasma). As the power is increased towards the critical power for ring creation, the linewidth of the central spot narrows by a factor of two, becomes more symmetric (not shown), and less red shifted compared to the central spot at lower density. Since the line is symmetric and narrow, we believe this to be the natural emission of a gas of excitons. At excitation powers just above the critical power for ring creation, the spectra of both the ring and the central spot remain narrow and symmetric, and remain roughly at the same energy (see also Figure 2h). As the power is further increased and the radius of the ring grows, the spectrum of the central spot red shifts, broadens, and becomes asymmetric (see also fig 2i), indicative of a gas of dissociated carriers again. In contrast, the spectrum of the ring remains nearly constant: unshifted, symmetric, and narrow, indicative of a gas of excitons. Finally, Figure 3d plots the peak PL intensities as a function of power. The center spot emission increases with power, except for a sudden drop around the threshold for ring creation. The ring intensity, on the other hand, drops with increasing power (and corresponding increasing radius).

We now try to construct a consistent physical picture to account for all of our experimental results. Figure 4a shows a schematic description of the relevant processes associated with above-the-barrier photoexcitation, under an applied bias in the growth direction. Without photoexcitation, a 2D electron gas is present in the QW due to the modulation doping of the sample (this is likely to be true even for the samples of Ref. [1] when under bias). Applying bias will change the electron density in the QW and generate a leakage current. When hot electrons and holes are photogenerated by the laser, as shown by the red and blue dots in Figure 4a, they can either drift under the applied bias to the contacts or cool down through phonon-carrier or carrier-carrier scattering, and consequently get trapped in the QW (red and blue open circles). However, the trapping rate of holes is expected to be larger than that of the electrons. This can be attributed to several factors: First, the hole has a much smaller drift velocity (mobility) than the electron, by a factor of 10-20 [6], so it takes longer for the hole to drift away from the QW, and thus it has a higher probability of scattering into the QW. Secondly, the phonon scattering time of the holes is much shorter than that of the electrons [7]. This results in the hot holes cooling faster (and drifting slower). As a consequence, there is an excess of photogenerated holes that end up trapped in the QW.

These holes will recombine with the electron gas in the QW, thus depleting it. The degree of depletion depends on the photogeneration rate compared to the leakage rate from the contacts which can replenish the electron density. With high enough excitation power, the electron gas can be almost completely depleted, leaving a population of trapped cold holes instead. Since the illumination area is small, the optically induced depletion of electrons and the accumulation of the holes in the QW plane is local. As a result, close to the center spot, there will be a puddle of holes, surrounded by a sea of electrons. Due to diffusion, the holes tend to spread outwards, while the electrons will flow inwards. This process is schematically shown in Figure 4b. In steady state, the holes and electrons are spatially separated in the plane of the QW, *perpendicular* to the applied electric field, forming a sharp (nominally circular) boundary which extends to a radius larger than that of the excitation spot. Since electrons and holes can only recombine where they meet, a sharp luminescence ring will form at the boundary between the two regions of opposite charges.

With this physical picture, the dynamics of the carriers in the QW plane can be described using the following coupled rate equations:

$$\frac{\partial n_{hot}}{\partial t} = D_{hot}^e \nabla^2 n_{hot} - \frac{n_{hot}}{\tau_{cool}^e} - \frac{n_{hot}}{\tau_{drift}^e} + Af(r) \quad (1)$$

$$\frac{\partial p_{hot}}{\partial t} = D_{hot}^h \nabla^2 p_{hot} - \frac{p_{hot}}{\tau_{cool}^h} - \frac{p_{hot}}{\tau_{drift}^h} + Af(r) \quad (2)$$

$$\frac{\partial n_{cold}}{\partial t} = D_{cold}^e \nabla^2 n_{cold} + \frac{n_{hot}}{\tau_{cool}^e} - \frac{n_{cold} - n_{eq}}{\tau_{leak}^e} - \xi n_{cold} p_{cold} \quad (3)$$

$$\frac{\partial p_{cold}}{\partial t} = D_{cold}^h \nabla^2 p_{cold} + \frac{p_{hot}}{\tau_{cool}^h} - \frac{p_{cold}}{\tau_{leak}^h} - \xi n_{cold} p_{cold} \quad (4)$$

The first two equations describe the dynamics of the density distributions of hot electrons $n_{hot}(\vec{r})$ and hot holes $p_{hot}(\vec{r})$ in the plane. Here, the first term on the right hand side of these equations allows the hot electrons and holes to diffuse with diffusion constants D_{hot}^e and D_{hot}^h (the ∇^2 are derivatives in the in-plane directions only). The next two terms on the right hand side allow the hot electrons and hot holes to cool with characteristic times τ_{cool}^e and τ_{cool}^h respectively or to drift to the contacts with times τ_{drift}^e and τ_{drift}^h . Finally, we have added the source term $Af(r)$ which creates hot electrons and holes from photons. Here, $f(r)$ is the normalized excitation beam profile and A is the total absorbed photon flux (each absorbed photon generates one electron and one hole).

Similarly, the third and fourth equations describe the dynamics of the density distributions of cold electrons $n_{cold}(\vec{r})$ and cold holes $p_{cold}(\vec{r})$ in the plane. Again, the first term on

the right hand side allows the cold electrons and holes to diffuse with diffusion constants D_{cold}^e and D_{cold}^h . The second term on the right hand side generates cold carriers from any hot carriers that are cooled down. The third term on the right hand side allows the cold electrons and cold holes to leak to or from the contacts with rates τ_{leak}^e and τ_{leak}^h respectively, in a way that tries to bring the densities back to the (equilibrium) densities of the dark state (n_{eq} for electrons, and zero for holes). Finally, the last term on the right hand side represents the recombination of cold electrons and cold holes, where ξ is the electron-hole capture (or collision time) coefficient. Note that we have written this term as being proportional to the product $n_{cold} p_{cold}$ which assumes that the rate limiting step in recombination is the rate for the electron and the hole to find each other and form a pair, *i.e.*, we have assumed that once an electron-hole pair is formed, it will recombine immediately. Note also that the intensity of emission is given by the number of electrons and holes that recombine and hence the spatial profile of emission is given by the spatial dependence of the product $n_{cold} p_{cold}$.

Although there are many parameters in this model, all of them are known or can at least be estimated. A detailed discussion of all these parameters is given in the methods section below. Further simplification of these equations can be made by neglecting the diffusion of hot carriers in the plane. This is a reasonable assumption because in-plane diffusion is typically much slower than the drifting and cooling processes. Under these assumptions, the equations for the hot carriers can be solved exactly. This reduces the problem to a set of only two coupled rate equations for the cold carriers (see methods section below).

The steady state solutions of the model are presented in Figure 5 for the set of parameters discussed in the methods section below at an excitation power level where a ring is formed. The laser intensity profile is shown in by the black dotted line. The in-plane cold electron and hole density distribution profiles are shown by the red and blue lines, respectively. Consistent with our qualitative picture, the model predicts that both the electron depletion region and the puddle of holes are larger than the excitation spot due to the diffusion processes. The olive line shows the emission profile, which is just the product of the cold electron and cold hole densities. The emission ring appears at the sharp boundary between the electron sea and the hole puddle. The calculated emission patterns corresponding to the experimental conditions of Figure 2a-c are plotted in Figure 2d-f. There is a good agreement between the experiment and calculation except for the experimental asymmetry of the ring with respect to the center spot. We attribute the asymmetry of the ring to a gradient of barrier width,

which for simplicity is not taken into account in our model. As the barrier width changes there will be corresponding changes in n_{eq} causing the ring radius to locally vary.

In order to check the validity and consistency of our model, we compare its predictions to our spectroscopic experimental findings in Figure 3. First, as the excitation power is increased above a threshold, the electron depletion region and the area of the hole puddle increase. This pushes the ring out and away from the center spot. This behavior is well reproduced by the model, as seen in Figure 3e. The second crucial test of our physical picture is its ability to explain the puzzling dependence on excitation power of the linewidth and energy of the PL of the center spot. It is well known that the emission linewidth of a 2D electron-hole gas is a measure of the holes and electron Fermi energies which are determined by their corresponding densities (n_{cold} and p_{cold}). Figure 3f shows the calculated linewidth (γ) assuming a quasi-degenerate 2D electron-hole gas, and is given by $\gamma = E_f^e + E_f^h = \pi\hbar^2(n_e/m_e + n_h/m_h)$. Here, E_f^e and E_f^h are the electron and hole Fermi energies, and m_e and m_h are the electron and hole effective masses, respectively. The energy shift due to bandgap renormalization also depends on n_{cold} and p_{cold} : the larger the total carrier density, the larger the emission red-shift due to carrier-carrier correlations. Following Ref. [8, 9], the bandgap renormalization is approximated by $E_{BGR} = E_0 - \eta(n_{cold} + p_{cold})^{1/3}$, with η a fit parameter, and is plotted in Figure 3g. Here, E_0 is the QW transition energy (at zero density) and η is a fitting parameter. Both the calculated linewidth and energy shift agree well with the experimental results. Finally, Figure 3g plots the calculated peak intensity of the center spot and ring PL as a function of power. As with the previous dependencies, it agrees well with the experimental behavior shown in Figure 3d.

In addition to the above described quantitative agreement of the experiment and the model, it is also very easy to understand how the qualitative trends come about. At low excitation power, we do not generate enough cold holes to substantially deplete the existing cold electron density (estimated to be $10^{11}cm^{-2}$ from PL linewidth). Thus, we should see PL corresponding to recombination in the presence of a high density of free charge carriers which should be broad, red-shifted, and asymmetric, as we indeed observe (see Figure 2g). Increasing excitation power, the depletion of electrons becomes more significant, leading to a reduction of the excess electron density with only a small increase of holes. This lower density leads to a decrease in linewidth and a smaller red-shift of the center spot. As the power is further increased, the center spot is completely depleted of electrons and

the ring starts to appear. At this point, the total carrier density at the center is around $2 \times 10^{10} \text{cm}^{-2}$, and correspondingly the spectral lines are narrower and less redshifted (see Figure 2h). Increasing the power still further will start to build up a large hole density in the center spot. The increase in charge carriers in the center spot then reverses the previous trend making the central spot once again broad, asymmetric, and redshifted (see Figure 2i). In contrast, the total carrier density at the ring (estimated to be $\sim 2 \times 10^{10} \text{cm}^{-2}$) remains nearly independent of the excitation power, and therefore no change in its linewidth and energy position is observed. At this low density, the emission from the ring appears excitonic.

The ability of our model to describe the various experimental results strongly supports the validity of the physical picture presented above. The agreement of the experiment and theory is impressive — particularly given the very crude nature of the theoretical model. Furthermore, the qualitative trends of the model are quite independent of the precise values of the input parameters.

We are now in a good position to answer the questions posed at the beginning of this paper. According to our model, the particles that are being transported are free carriers and no additional excitonic transport mechanism is necessary in order to explain our experimental data. Nonetheless, it seems that the ring emission is due to excitonic recombination (as is the center spot for excitation powers close to the threshold power for ring creation). The actual thermodynamic state of the exciton gas in the ring remains a very interesting open question. It was hypothesized in Refs. [1, 2] that the exciton gas is statistically degenerate. This is not excluded by our model (see also the discussion below). In fact, our model predicts a carrier density of $\sim 2 \times 10^{10} \text{cm}^{-2}$, which is of the order of the Kosterlitz-Thouless 2D transition density to a superfluid state at $T=2\text{K}$. (The data of Figure 2 and 3, however, are performed at higher temperatures). As for the driving force, diffusion of free carriers seems to sufficiently account for the observed effects. At first glance, it might seem that the carrier-carrier Coulomb interaction should play an important role. However, since the distance of the GaAs n^+ conducting layers from the 2D gas layer is very small, any long range Coulomb interactions will be screened out, although plasmons can still propagate, which may be important for understanding the short time behavior reported in Ref. [3]. Furthermore, the Coulomb term may be important in understanding the pattern formation which occurs at very low temperatures, reported in Ref. [1]. In particular, below $T=1.8\text{K}$, the luminescence ring breaks into a periodic bead-like structures, which could possibly be

understood as pattern formation arising from competition between repulsion of like charges and attraction of opposite charges.

While our model explains the experiments described here and in Ref. [2, 3] quite well, there are few points left unresolved. First, the observed saturation of the center spot linewidth and energy shift at very high excitation powers cannot be reproduced by our simple model. At such high powers, other effects not included in our model, such as heating and charge buildup, can become significant. Furthermore, the model can only partially account for the results in Ref. [1]. For example, neither our experiments nor our model calculations show any clear evidence of the inner ring seen by Butov et. al. which may be related to the inability of excitons to recombine until they have cooled to energies within the light-cone[1].

Another point worth mentioning is the dependence of the ring PL spatial sharpness with temperature. The model predicts that the ring width increases with increasing particle capture time, which also agrees with the observation that the ring broadens as the temperature is raised. (In the methods section we describe how the particle capture time is estimated). However, other parameters, such as the time constants, may also be temperature dependent making quantitative comparisons difficult at this stage.

A very intriguing prediction of the model is that the macroscopic charge separation and therefore the ring emission persists for an extremely long time compared to the center spot lifetime after the laser excitation is turned off. This behavior is shown in Figure 6, where the ring lifetime is longer than $1\mu s$. In comparison, the center spot decays after less than $1ns$. While the center spot lifetime is determined by the free carrier recombination time, the ring lifetime is determined by a slow carrier diffusion, which is driven by the carrier density gradients in the plane. This long lifetime of the ring is consistent with time-resolved measurements presented in Ref. [2], which reported a ring PL lifetime longer than $260ns$. This long lifetime suggests that excitons being formed in the ring should be well thermalized because the carriers should have had plenty of time to cool over the long time from their hot optical creation. We suggest that this should be a very good method of forming cold excitons, opening up opportunities for studying their quantum statistics at low temperatures.

Methods

With the above mentioned approximation that diffusion of hot carriers can be neglected, in steady state the reduced set of couple equations are simply Eq. 3 and Eq. 4 where

$n_{hot}/\tau_{cool}^e = C_e Af(r)$ and $p_{hot}/\tau_{cool}^h = C_h Af(r)$ with $C_{e(h)} = 1/(1 + \tau_{cool}^{e(h)}/\tau_{drift}^{e(h)})$. The ratio between the hot carrier cooling time and drifting time, $C_e(h)$, can be estimated by comparing the experimentally measured light induced electric current to the number of photogenerated hot carriers, which is determined by the number of photons absorbed in the QW structure. We use $C_e \cong 0.2$ and $C_h \cong 1$. We use a gaussian beam profile ($f(r)$) to describe our excitation spot with a beam diameter of $60\mu m$ FWHM. The typical photon flux absorbed is $2 \times 10^5 ns^{-1} \mu m^{-2}$. ξ , the capture coefficient, is estimated by a simple, classical free electron-hole Coulomb capture model. In this model, a charged carrier is assumed to be captured by an opposite charge if its thermal kinetic energy is smaller than the coulomb attraction. This model results in a capture cross section of $\sigma = \frac{e^2}{6\pi\epsilon kT}$. ξ is then given by $\sigma v_{th}/d = \frac{e^4}{36\pi\epsilon^2 d} \sqrt{\frac{3}{\mu^* k^3 T^3}}$ where v_{th} is the thermal velocity of the carrier, μ^* is the reduced electron-hole effective mass, and d is the thickness of the QW. The electron-hole pair capture time is typically much longer than the recombination time at all the experimental carrier densities. For example, at a carrier density of 10^{11} , the capture time is 1ns. Therefore, the assumption that ξ is limited by the capture time is well justified. Although this calculation is quite crude, the calculated capture time is also consistent with the luminescence rise time of the center spot which was measured to be $\sim 1ns$ [2]. The diffusion coefficient for the electrons is calculated from the measured electron mobility of the structure to be $D_e = 20\mu m^2/ns$ and that of the holes is then inferred to be $D_h = D_e m_e/m_h = 5\mu m^2/ns$. The leakage time τ_{leak} is taken to be on the order of $10\mu s$, and $n_{eq} = 10^{11}/cm^2$.

Acknowledgement

This work has been partially supported by the National Science Foundation and the Department of Energy. We thank Phil Platzman, Girsh Blumberg, Nikolai Zhitenev, Rafi de Picciotto, Chandra Varma and Peter Littlewood for helpful discussions.

Competing interests statement

The authors declare that they have no competing financial interests.

Correspondence and requests for materials should be addressed to S. H. S. (email: shsi-

- [1] Butov, L. V., Gossard, A. C. & Chemla, D. S. Macroscopically ordered state in an exciton system. *Nature* **418**, 751–754 (2002).
- [2] Snoke, D., Denev, S., Liu, Y., Pfeiffer, L. & West, K. Long-range transport in excitonic dark states in coupled quantum wells. *Nature* **418**, 754–757 (2002).
- [3] Snoke, D., Denev, S., Liu, Y., Pfeiffer, L. & West, K. Luminescence rings in quantum well structures. *Solid State Comm.* **127**, 187–196 (2003).
- [4] Kukushkin, I. V., von Klitzing, K., Ploog, K., Kirpichev, V. E. & Shepel, B. N. Reduction of the electron density in GaAs-Al_xGa_{1-x}As single heterojunctions by continuous photoexcitation. *Phys. Rev. B* **40**, 4179–4182 (1989).
- [5] Ramon, G. *et al.* Scattering of polaritons by a two-dimensional electron gas in a semiconductor microcavity. *Phys. Rev. B* **65**, 085232 (2002).
- [6] Adachi, S. (ed.). *Properties of Aluminum Gallium Arsenide* (INSPEC, the Institute of Electrical Engineers, London UK, 1993).
- [7] Shah, J. *Hot Carriers in Semiconductor nanostructures: Physics and Applications* (Academic Press, New York, 1992).
- [8] Tränkle, G. *et al.* General relation between band-gap renormalization and carrier density in two-dimensional electron-hole plasmas. *Phys. Rev. B* **36**, 6712–6714 (1987).
- [9] Schmitt-Rink, S., Ell, C., Koch, S. W., Schmidt, H. E. & Haug, H. Subband-level renormalization and absorptive optical bistability in semiconductor multiple quantum well structures. *Solid State Comm.* **52**, 123–125 (1984).
- [10] Adachi, S. GaAs, AlAs, and Al_xGa_{1-x}As Material parameters for use in research and device applications. *J. Appl. Phys.* **58**, R1–R29 (1985).

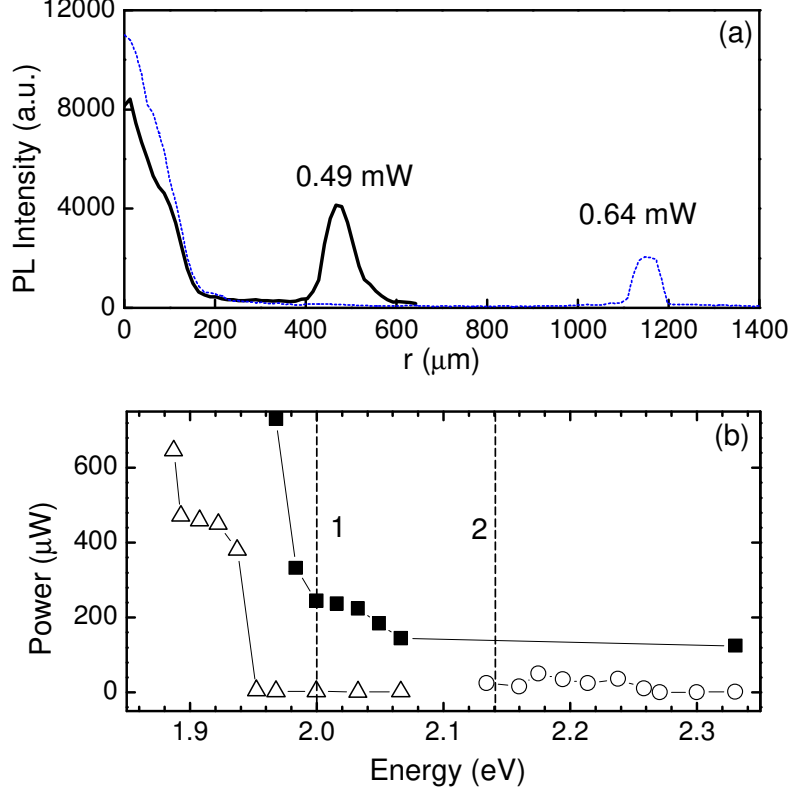


FIG. 1: (a) Example of the luminescence ring for a double quantum well structure (Structure A, see below) similar to the one used in Ref. [2] for two different laser powers. The sample was measured at $T=2\text{K}$, and excited with a HeNe laser (632 nm) with a spot diameter of $\sim 100\mu\text{m}$ at $r = 0$. (b) Laser power threshold for the formation of the ring as a function of the excitation energy. This plot shows that the ring forms easily only for excitation energies above the bandgap of the barriers. For samples A and B (solid squares and open triangles, respectively) the bandgap of the barriers (2.0 eV) is marked by vertical line 1. For excitation energies below this threshold, a ring can be formed only by using much larger laser power. For sample C (open circles) the bandgap of the barriers (2.15 eV) is marked with vertical line 2. For this sample, no ring was observed for excitation energies below 2.13 eV. In samples A and B no ring was observed for any excitation power for excitation energies below 1.88 eV. Structure A (solid squares) consists of two 60 \AA $\text{In}_{0.1}\text{Ga}_{0.9}\text{As}$ quantum wells, separated by a 40 \AA GaAs barrier, with 300 and 1000 \AA $\text{Al}_{0.32}\text{Ga}_{0.68}\text{As}$ outer barriers separated from the wells by 50 \AA GaAs buffer layer. Structure B consists of two 80 \AA GaAs quantum wells, separated by a 40 \AA AlAs barrier, with 2000 \AA $\text{Al}_{0.33}\text{Ga}_{0.67}\text{As}$ outer barriers, which is the same design as used in Ref. [1]. Structure C (open circles) is the same as structure A, but with $\text{Al}_{0.44}\text{Ga}_{0.56}\text{As}$ outer barriers. Values for bandgaps are taken from Ref. [10].

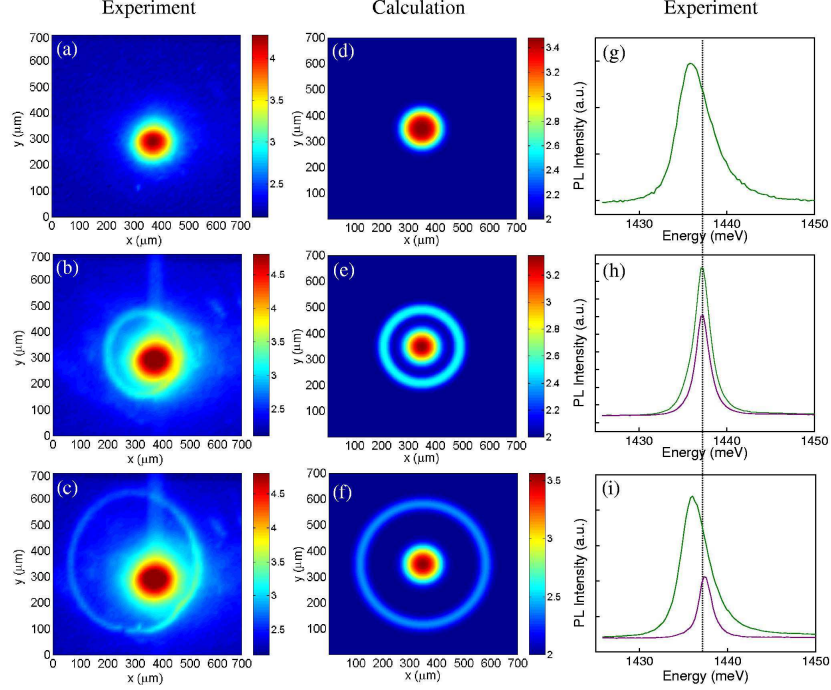


FIG. 2: Photoluminescence images for our single quantum well sample taken at three different excitation powers, 50, 265 and 296 μW , are shown in the left panel (a)-(c). A ring emission pattern forms when the power is larger than a threshold. The middle panel (d)-(f) shows the results of the model calculations based on a photo-induced, in-plane charge separation (see text). The parameters used for the calculations are discussed in details in the methods section. The asymmetry of the ring pattern with respect to the center spot is probably due to a gradient of the barrier width, which is not taken into account in our model. The right panel (g)-(i) presents the experimentally observed center spot (olive) and ring (purple) emission spectra. In (g) and (i) we see a broadening and a red-shift of the center spot which indicates a high density of carriers compared to the center spot in (h) and to the ring in (h) and (i). The sample was measured at $T=12K$, and excited with a HeNe laser (632 nm) with a spot diameter of $\sim 60\mu m$. Our sample consists of a single 60Å $In_{0.13}Ga_{0.87}As$ quantum well surrounded by $GaAs/Al_{0.32}Ga_{0.68}As$ 50Å/1000Å barriers. A 1000 Å layer of Si doped $GaAs$ is located 2000 Å from the QW on the n^+ substrate side and another similar layer is located 1000Å from the QW on the top contact side. See Figure 4a for a schematic diagram of the QW structure. Gold films are deposited on both sides of the sample to form contacts for applying bias. A 3mm hole is opened on the top gold film for the optical measurements.

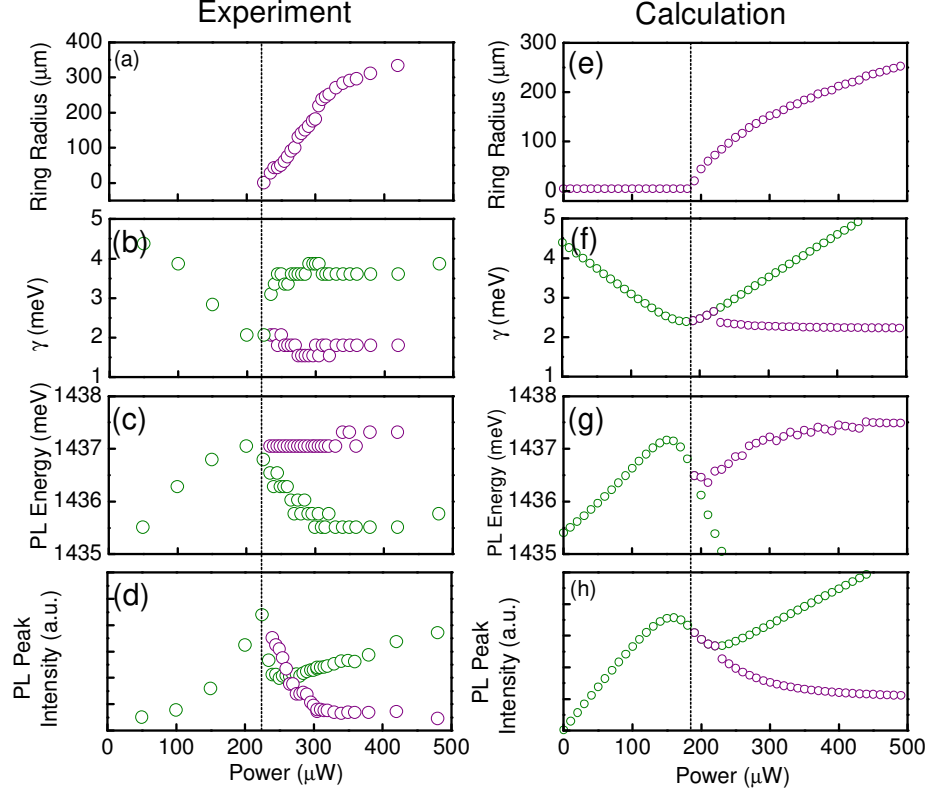


FIG. 3: Comparison between the experimental and model calculated excitation power dependences: (a) experimental and (e) calculated ring radius. The ring radius increases sublinearly after the excitation power reaches beyond a certain threshold. (b) the linewidth and (c) the energy of the center spot luminescence (olive circles) and the ring luminescence (purple circles). (f) Model calculated linewidth of the luminescence of the center spot and ring assuming degenerate 2D electron-hole plasma. (g) Model calculated energies of the center spot and ring luminescence based on bandgap renormalization. (d) Experimental and (h) calculated PL peak intensity at the center spot and the ring. Vertical dashed lines mark the onset of the ring formation. Note: The ring radius is always measured in the -y direction.

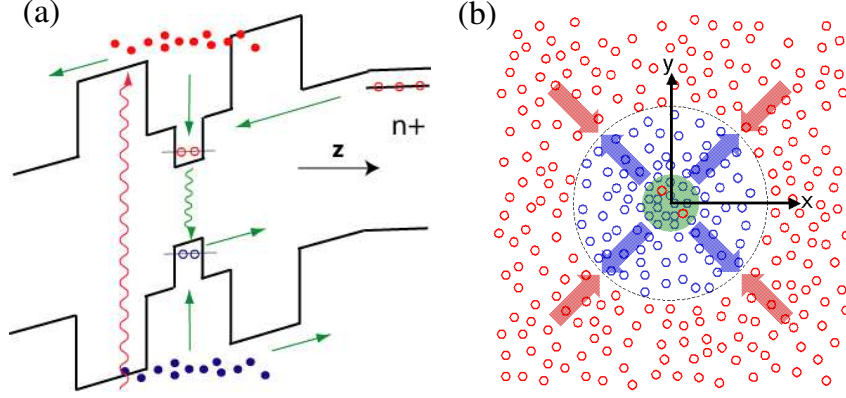


FIG. 4: (a) schematically describes the energy profile of the quantum well structure in the growth direction. Without light, the quantum well contains a 2D electron gas due to modulation doping with a density, and leakage current that depends on the bias. In our model, hot electrons (red solid circles) and holes (blue solid circles) generated by light with an energy above the barriers can either drift to the contacts or cool to become trapped in the quantum well (cold carriers - open circles). The hot holes have a higher probability of cooling down than hot electrons (see text). The excess of cold holes can recombine with the cold electrons leading to a depletion of cold electrons and accumulation of cold holes at the excitation spot. Cold electrons and cold holes can also leak to/from the contacts in this model. (b) Excess cold holes (open blue circles) built up near the excitation spot (shaded circular area) diffuse outwards while the cold electrons (open red circles), present in the absence of photoexcitation, far from the the excitation spot, diffuses inward. A sharp boundary (dotted circle) is formed between the hole puddle and the sea of electrons surrounding it. The recombination of electrons and holes at the boundary gives rise to the ring pattern. There is also a low density of photoexcited electrons in the center spot which quickly recombine with holes.

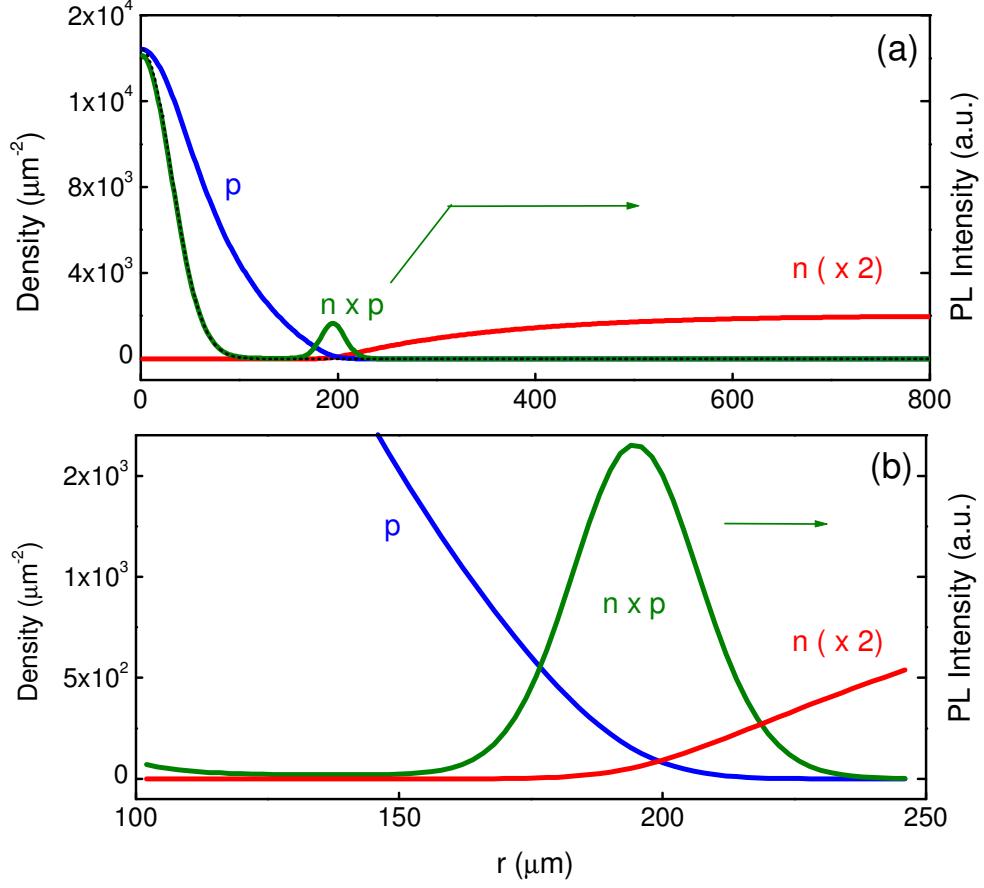


FIG. 5: (a) Model calculation for a continuous-wave excitation at a power of $350\mu W$. The black dotted line shows the incident photon intensity radial profile. The red and blue lines show the cold electron and cold hole density radial profiles, respectively. The electron depletion and hole accumulation regions are clearly seen to be larger than the excitation spot. The photoluminescence intensity profile, which is proportional to the product of the cold electron and cold hole densities, is plotted in olive. The ring emission pattern forms at the boundary between the puddle of cold holes and the sea of electrons. (b) is a expanded view of (a) around the ring position.

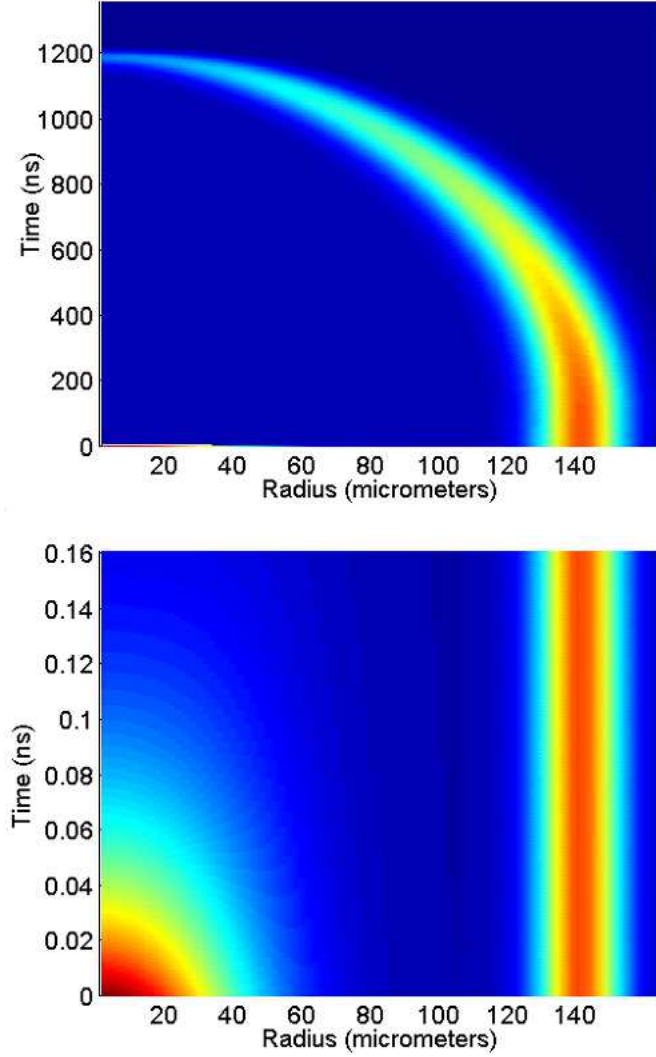


FIG. 6: (a) Calculated emission pattern cross section as a function of time after the excitation power is turned off. The ring emission intensity as well as its radius decay on a time scale of a microsecond. (b) An expanded view of (a) for very short times immediately after the power is turned off. The center spot decays in a typical recombination time of $\sim 50ps$, whereas the ring emission is very robust and persists for more than a microsecond after the excitation power is turned off. This time dependence of our model is in agreement with the experimental time behaviors reported in Ref. [2]